



UNIVERSIDADE ESTADUAL DE CAMPINAS  
SISTEMA DE BIBLIOTECAS DA UNICAMP  
REPOSITÓRIO DA PRODUÇÃO CIENTÍFICA E INTELLECTUAL DA UNICAMP

**Versão do arquivo anexado / Version of attached file:**

Versão do Editor / Published Version

**Mais informações no site da editora / Further information on publisher's website:**

<https://pubs.acs.org/doi/abs/10.1021/acs.jpca.6b05368>

**DOI: 10.1021/acs.jpca.6b05368**

**Direitos autorais / Publisher's copyright statement:**

©2016 by American Chemical Society. All rights reserved.

DIRETORIA DE TRATAMENTO DA INFORMAÇÃO

Cidade Universitária Zeferino Vaz Barão Geraldo

CEP 13083-970 – Campinas SP

Fone: (19) 3521-6493

<http://www.repositorio.unicamp.br>

# Kinetic Energy Release of the Singly and Doubly Charged Methylene Chloride Molecule: The Role of Fast Dissociation

K. F. Alcantara,<sup>†</sup> A. B. Rocha,<sup>§</sup> A. H. A. Gomes,<sup>||</sup> W. Wolff,<sup>‡</sup> L. Sigaud,<sup>⊥</sup> and A. C. F. Santos<sup>\*,‡</sup>

<sup>†</sup>Instituto Nacional de Tecnologia, 20081-312 Rio de Janeiro, RJ, Brazil

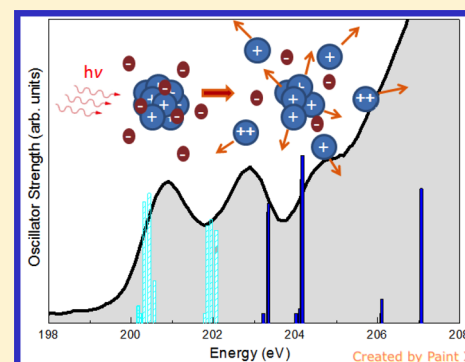
<sup>‡</sup>Instituto de Física, Universidade Federal do Rio de Janeiro, 21941-972 Rio de Janeiro, RJ, Brazil

<sup>§</sup>Instituto de Química, Universidade Federal do Rio de Janeiro, 21941-909 Rio de Janeiro, RJ, Brazil

<sup>||</sup>Instituto de Física Gleb Wataghin, Universidade Estadual de Campinas, 13083-859 Campinas, SP, Brazil

<sup>⊥</sup>Instituto de Física, Universidade Federal Fluminense, 24210-346 Niterói, RJ, Brazil

**ABSTRACT:** The center of mass kinetic energy release distribution (KERD) spectra of selected ionic fragments, formed through dissociative single and double photoionization of  $\text{CH}_2\text{Cl}_2$  at photon energies around the Cl 2p edge, were extracted from the shape and width of the experimentally obtained time-of-flight (TOF) distributions. The KERD spectra exhibit either smooth profiles or structures, depending on the moiety and photon energy. In general, the heavier the ionic fragments, the lower their average KERDs are. In contrast, the light  $\text{H}^+$  fragments are observed with kinetic energies centered around 4.5–5.5 eV, depending on the photon energy. It was observed that the change in the photon energy involves a change in the KERDs, indicating different processes or transitions taking place in the breakup process. In the particular case of double ionization with the ejection of two charged fragments, the KERDs present have characteristics compatible with the Coulombic fragmentation model. Intending to interpret the experimental data, singlet and triplet states at Cl 2p edge of the  $\text{CH}_2\text{Cl}_2$  molecule, corresponding to the Cl ( $2p \rightarrow 10a_1^*$ ) and Cl ( $2p \rightarrow 4b_1^*$ ) transitions, were calculated at multiconfigurational self-consistent field (MCSCF) level and multireference configuration interaction (MRCI). These states were selected to form the spin–orbit coupling matrix elements, which after diagonalization result in a spin–orbit manifold. Minimum energy pathways for dissociation of the molecule were additionally calculated aiming to give support to the presence of the ultrafast dissociation mechanism in the molecular breakup.



## I. INTRODUCTION

After the absorption of a sufficiently high-energy photon by methylene chloride, the excess of energy of the dissociating molecule is spread mostly among the fragments rather than inducing the fluorescence emission, because the molecule is made of light atoms (H, C and Cl). The excited molecular states prompted by the photoabsorption can follow several fragmentation pathways producing moieties with distinct translational energies following the rules of the fragmentation dynamics, obeying momentum and energy conservation laws. In this context, KER analysis, constituting a probe of the molecular fragmentation of the charged system, is of basic interest for understanding the structures of the moieties concerning the fragmentation dynamics and provides information on the excited states, on the character of repulsive states in the fragmentation process, and on the electronic states and potential energy functions.<sup>1–3</sup>

The goal of this work is to obtain the average kinetic energies and KERD of several ionic fragments resulting from the dissociative photoionization of the singly and doubly charged  $\text{CH}_2\text{Cl}_2$  molecule, as extracted by time-of-flight spectra. It is well-known that in time-of-flight (TOF) mass spectra the peak width of the parent molecular ion is composed by the thermal

velocities and spatial distribution of the target species, convoluted with an instrumental broadening due to electronics.<sup>4</sup> On the other hand, for the breakup channels, ions resulting from molecular fragmentation depict mostly TOF peak profiles broadened by the changeover of the dissociation energy into kinetic energy release (KER) and the momentum distribution between a two- and a three-body breakup. It should be pointed out that although the energy distributions of the charged fragments can be determined, the total energy distribution cannot be ascertained when neutral fragments are involved in the breakup channels carrying part of it. Notwithstanding, KERDs of molecular fragments have to be interpreted with caution due to the internal energy of the fragments.

The selected molecule in this study, dichloromethane (DCM), is amply employed as a paint stripper, degreaser, and agent to decaffeinate coffee and tea. Its high volatility is useful as an aerosol spray propellant as well as a blowing agent for polyurethane foams.<sup>5–7</sup> DCM is an atmospheric trace gas

**Received:** May 30, 2016

**Revised:** August 8, 2016

**Published:** August 15, 2016



with a tropospheric lifetime of about 150 days and comes from major anthropogenic sources.<sup>5–7</sup> Atmospheric concentrations of DCM peaked around 1990 and have declined during the first years of this century. However, new observations indicate that DCM has been increasing in the atmosphere.<sup>8</sup> The fragmentation of DCM induced by EUV, soft X-rays, solar wind, and galactic cosmic rays has been related to the depletion of the ozone layer.<sup>5–7</sup> In previous work, a comparative study for the fragmentation of the DCM molecule was performed for collisions of fast protons and EUV photons.<sup>9</sup> It was shown that the larger is the proton energy, the more the fragmentation pattern resembles the corresponding photoionization yield at lower energies. In another work,<sup>10</sup> the photoionization of the dichloromethane molecule was studied for photons with energies in the soft energy range. It was found that the electronic de-excitation gives rise to one to three electrons and an ionic molecule that decays into smaller moieties through several fragmentation channels. The chlorine ion, Cl<sup>+</sup>, had the highest intensity around and above the Cl 2p edge, while the CH<sub>2</sub>Cl<sup>+</sup> ion, corresponding to the loss of one neutral chlorine atom, dominated the mass spectra in the valence region. In addition, strong electronic selectivity was observed for the core-excited molecule. Moreover, the roles of the shake-off and knockout processes in the double photoionization of the DCM molecule were also studied.<sup>11</sup> The probabilities for both mechanisms accompanying valence-shell photoionization were estimated as a function of incident photon energy using existing models from the literature. The experimental results are in qualitative agreement with the models.

The main mechanism related to the depletion of ozone is via reactions with chlorine atoms. Chlorine compounds can undergo dissociation, releasing a chlorine atom as the result of a collision process.<sup>9</sup> Atomic chlorine is highly reactive and breaks ozone molecules, forming a chlorine monoxide and an oxygen molecule. Chlorine monoxide, in turn, can react with either an oxygen atom or another ozone molecule, resulting in a chlorine atom and one or two oxygen molecules, respectively, leading to a feedback reaction mechanism where a single chlorine atom can break down a large number of ozone molecules. This work explores the formation of singly and doubly charged fragments from Cl<sub>2</sub>H<sub>2</sub> around the Cl 2p edge. Although the X-ray cross sections are small in comparison to the corresponding UV or VUV processes, the damage due to the former is much higher, affecting the equilibrium distribution of ions in the ionosphere. Thus, a detailed study of the controlling chemical processes is essential for an appropriate comprehension of ionospheric composition and behavior.

## II. EXPERIMENTAL SECTION

The experimental apparatus has been reported previously,<sup>10–13</sup> and only a brief description is included here. The CH<sub>2</sub>Cl<sub>2</sub> molecule was photoionized by soft X-rays from the LNLS synchrotron radiation facility monochromatized in the TGM beamline (energy resolution: 500 < E/ΔE < 700). The photoionization products of CH<sub>2</sub>Cl<sub>2</sub> were separated according to their mass-to-charge ratio by a time-of-flight (TOF) mass spectrometer, using the ejected electrons and the cations as start and stop signals, respectively, for a time to digital converter (TDC). From these TOF profiles, the KERD of several cations were deduced for several photon energies. The extraction field chosen for the spectrometer in the experiment is high enough (7000 V/m) to guarantee 100% collection efficiency for ions up to 30 eV.<sup>11</sup> The experiment was

accomplished using an effusive gas jet at room temperature. Although the arising thermal energies might influence the TOF profiles, they are a minor factor compared to the released energies. The TOF distribution of the singly ionized parent molecules is described by a Maxwell–Boltzmann energy profile, which was also checked measuring argon gas spectra at room temperature.

The KERD of the CH<sub>2</sub>Cl<sub>2</sub> fragments were investigated in the energy range around the Cl 2p edge (195–215 eV) by means of the analysis of the TOF profiles through the PEnPICO technique. The mean kinetic energy release (KER) in the fragmentation process gives rise to a velocity spread of the fragment ions. This spread can be tracked by measuring the TOF distributions of the fragments. The time-of-flight peak profiles allow us to compute the average kinetic energy release measurements<sup>4</sup> of the coincidence products of the CH<sub>2</sub>Cl<sub>2</sub> molecule. Since the fragments are space focused and the electric field in the interaction region is uniform, the mean KER in the fragmentation process, ⟨U⟩, can be calculated from the peak fwhm through the formula<sup>4,12</sup>

$$\langle U \rangle = \left( \frac{qE\Delta t_{\text{FWHM}}}{2} \right)^2 \frac{1}{2m} \quad (1)$$

where  $q$  is the ion charge state,  $E$  is the electric field in the extraction region,  $\Delta t_{\text{fwhm}}$  is the peak width (fwhm), and  $m$  is the ion mass. The present mass resolution,  $m/\Delta m$ , is better than 200. The zero of the KERD scale was obtained from the position (peak maximum) of the fragment TOF profiles, assuming a symmetrical profile. Because the KERD is proportional to the square of  $\Delta t$ , the absolute precision of the energies,  $\delta U$ , is better for low KER ( $\delta U/U = 2\delta\Delta t/\Delta t = \Delta m/m < 5 \times 10^{-3}$ ), where  $\delta\Delta t$  is the time resolution. The kinetic energy distributions  $N(U)$  can be worked out from the shape of the lines  $I(t)$  observed in the TOFMS, through the relation

$$N(U) = \frac{2m}{(qE)^2} \left| \frac{dI(t)}{dt} \right| \quad (2)$$

In the case of the PE2PICO coincidences, the corresponding average KER and KERDs were extracted after projecting the coincidences islands onto the  $T_1$  and  $T_2$  axes,<sup>10</sup> which correspond to the time-of-flight of the first and second fragments to hit the detector, respectively.

## III. THEORETICAL APPROACH

In order to designate the transitions, which are responsible for the structures observed in the experimental results (the combined experimental and theoretical investigation is presented in detail in the Results and Discussion section), high-level ab initio quantum mechanical calculations were performed taking into account the spin–orbit coupling. Singlet and triplet states at Cl 2p edge of the CH<sub>2</sub>Cl<sub>2</sub> molecule, corresponding to the Cl (2p → 10a<sub>1</sub><sup>\*</sup>) and Cl (2p → 4b<sub>1</sub><sup>\*</sup>) transitions, were calculated in order to form a basis set of molecular states from which the spin–orbit splitting can be inferred. The method used was described previously.<sup>14</sup> In the present case, a total of 12 states are used to form spin orbit matrix element for each transition from a single chlorine atom. For instance, in Cl (2p → 10a<sub>1</sub><sup>\*</sup>) transition there are 3 singlet states (corresponding to transition from each 2p orbital), and consequently 9 triplets. That is why the spin–orbit manifold has 12 states for each chlorine atom. However, there are 2

chlorine atoms per molecule, which doubles the number of states (to 24), although the 12 uppermost lie high above the ionization threshold. So, one can effectively have up to 12 transitions from ground to Cl ( $2p \rightarrow 10a_1^*$ ) states and 12 more for Cl ( $2p \rightarrow 4b_1^*$ ). Initially, a multiconfigurational self-consistent field (MCSCF) calculation is performed in order to obtain orbitals averaged among ground and  $2p$ -core states, followed by multireference configuration interaction (MRCI) in order to establish a set of singlet and triplet states at the  $2p$  excitation edge. Then, the full Breit-Pauli Hamiltonian is formed and diagonalized on this state basis. The active space in the MCSCF step is composed of inner-shell  $2p$  orbitals of chlorine atoms and the corresponding unoccupied orbital in a state-averaged MCSCF, by considering only singly excited configurations for each state. This is a very simple wave function but it is able to take into account the most important effect of an inner-shell state, that is, the relaxation of the orbitals due to the formation of a core hole. The correlation effects are recovered by MRCI. With these eigenfunctions of the electronic Hamiltonian,  $H_{el}$ , the total Hamiltonian,  $H_{el} + H_{SO}$ , is diagonalized, where  $H_{SO}$  is the spin-orbit Hamiltonian in the full Breit-Pauli form.<sup>15–18</sup> Finally, the transition moment involving the ground state and the states of the spin-orbit manifold are calculated in order to determine the relative transition intensities. All calculations were done with the Molpro package<sup>19</sup> with Dunning's aug-cc-pVTZ-DK basis set. Scalar relativistic effects are taken into account by the Douglas-Kroll-Hess Hamiltonian up to third order in all steps of the calculation.

Minimum energy pathways for dissociation of the molecule were additionally calculated to support to the presence of the ultrafast dissociation mechanism in the molecular breakup. Potential energy curves were calculated, for some representative states, as a function of the C–Cl distance. For a given C–Cl distance, all other coordinates are optimized, meaning that this is a minimum energy path. For inner-shell states, such as Cl ( $2p \rightarrow 10a_1^*$ ), the inner-shell orbital is relaxed in the first step and then kept fixed for all points of the potential curve. This is done to avoid the variational collapse to a low-lying electronic state. All other orbitals are relaxed for each geometry optimization. For the ground state calculation, all orbitals are relaxed without restriction, since the problem of variational collapse does not apply. For these potential curves, calculations a smaller basis set was used, i.e., cc-pVDZ and spin-orbit effects were not taken into account.

#### IV. RESULTS AND DISCUSSION

Figure 1 shows the total ion yield spectrum of the  $\text{CH}_2\text{Cl}_2$  molecule around the Cl  $2p$  edge. Included in this figure are TOF profiles of the ionic isotopic chlorine atoms,  $^{35}\text{Cl}^+$  and  $^{37}\text{Cl}^+$ , at selected photon energies. These profiles were chosen to point out that changing the photon energy leads to a change in their shape and their width and, consequently, a change in the KERDs. The doublet structures in the Total Ion Yield (TIY) spectrum, at 200.7 eV (band A) and 202.8 (band B), are due to the spin-orbit (SO) splitting of the  $2p_{3/2}$  and  $2p_{1/2}$  levels of chlorine. Spin-orbit effects generally become apparent as energy splitting among states that exhibit similar electronic configuration. Even though molecular-field effects are characteristic of the chemical environment of the observed electron, molecular core levels are usually treated as atomic-like. These molecular-field effectiveness produce, among other outcomes, energy shifting in the core-level and valence orbitals. Thus, the

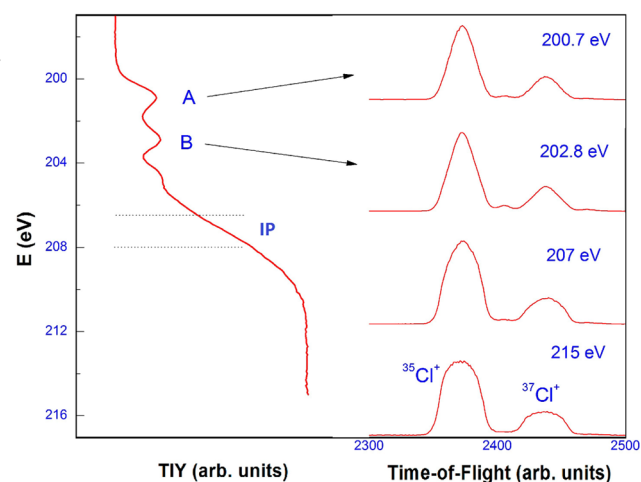


**Figure 1.** Left side: Total ion yield (TIY) of the  $\text{CH}_2\text{Cl}_2$  molecule as a function of the photon energy. Right side: Time-of-flight spectra of  $^{35}\text{Cl}$  and  $^{37}\text{Cl}$  at selected photon energies. See text for the peak designations (A,B) and dot lines explanations.

trend to treat molecular inner shells as essentially atomic-like is justified by the fact that molecular-field properties induce negligible perturbations on core-level spectra.

In Figure 1, total ion yield (TIY) of the  $\text{CH}_2\text{Cl}_2$  molecule as a function of the photon energy is shown. The assignment of the first two absorption bands, designated A and B, is done with the help of ab initio calculations in Figure 2. Band A is related

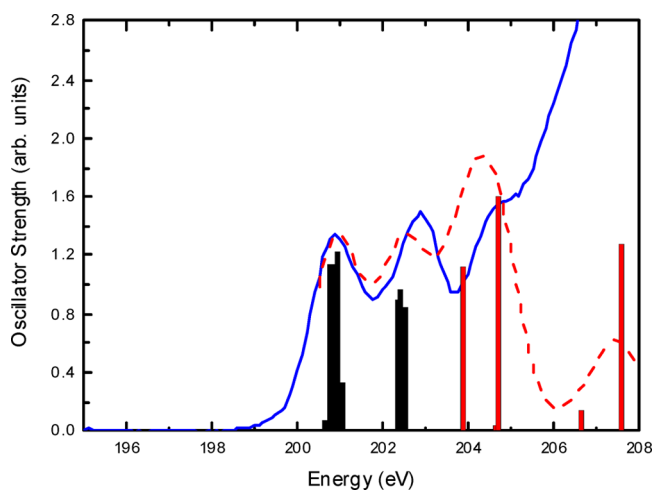


**Figure 2.** Transition intensities as a function of the photon energy. Full line: experimental data; black bars: theoretical calculation for the  $2p \rightarrow 10a_1^*$  transition; red bars: theoretical calculation for the  $2p \rightarrow 4b_1^*$  transition. Theoretical results were shifted by +0.5 eV in order to better fit the experimental spectra and a Gaussian function (dashed line) was fitted to each transition in order to reproduce the experimental line width from theoretical values.

to the transition Cl ( $2p_{3/2} \rightarrow 10a_1^*$  - 200.7 eV), in agreement with previous report,<sup>20</sup> while band B, to the Cl ( $2p_{1/2} \rightarrow 10a_1^*$  - 202.8 eV). The first transition to  $4b_1^*$  is around 204 eV ( $2p_{3/2} \rightarrow 4b_1^*$ ). The two ionization limits due to the spin-orbit splitting of the  $2p$  hole, Cl  $2p_{3/2,1/2} \rightarrow \infty$  (IP) are designated by the dotted lines at 206.4 and 208.0 eV,<sup>20</sup> respectively.

In Figure 2, the theoretical calculations and experimental results of the  $\text{CH}_2\text{Cl}_2$  molecule around the Cl  $2p$  edge are compared. Theoretical results were shifted by +0.5 eV in order

to better fit the experimental spectra and a Gaussian function was fitted to each transition in order to reproduce experimental line width from theoretical values, since they are obtained as expectation values and present no line width. The theoretical results essentially confirm the experimental assignment.

The total ion yield, after the subtraction of an offset due to contributions from valence shell ionization, has been normalized in order to compare with the theoretical transition intensities corresponding to the Cl ( $2p \rightarrow 10a_1^*$ ) and Cl ( $2p \rightarrow 4b_1^*$ ) transitions. Black bars stand for theoretical results for the  $2p \rightarrow 10a_1^*$  transition, where spin-orbit effects were taken into account as explained above, while red bars stand for theoretical calculations for the  $2p \rightarrow 4b_1^*$  transition. The ground state plus 24 L-Shell states were used to form the SO matrix. Therefore, there are 24 transitions from the ground to the excited states of the spin-orbit manifold. In some cases, the transition intensity vanishes. The main contributions are shown in Figure 2. The first transition lies around 200.7 eV and the last lies above 207 eV, i.e., inside the continuum of ionization of the 2p edge. If more states were used to form the SO matrix, the resulting states would lie still higher inside the continuum.

Calculations can highlight new information. For instance, for the  $2p \rightarrow 10a_1^*$  transition,  $2p_{3/2}$  components lie around 200.5 eV and  $2p_{1/2}$  components lie around 202 eV. There are components, instead of a single absorption, due to molecular splitting. If we take the center of the components as reference, the spin-orbit splitting is calculated as 1.51 eV, which is consistent, for instance, with the value calculated and measured for HCl.<sup>14</sup> It is worth mentioning that the experimental spectrum cannot assign the spin-orbit splitting since there is not enough resolution.

**IV.1. PEPICO Spectra.** In the range between 195 and 215 eV, the most abundant fragments in the mass spectra are  $\text{Cl}^+$  (31–44%),  $\text{H}^+$  (13–14%), and  $\text{CH}_2^+$  (9–16%), as listed in a previous work<sup>19</sup> and shown in Figure 3, as an example. Other breakups have been detected, but with relative intensities of less than 4%.

The KERD of these fragments and of the  $\text{C}^+$  fragment, corresponding to the full atomization of the molecule, were derived from the peak profiles of the TOF spectra. Figure 4

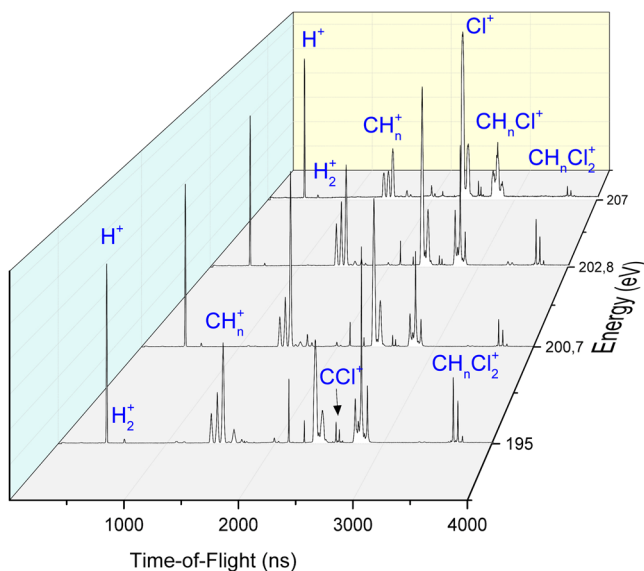


Figure 3. PEPICO spectra measured around the Cl 2p edge.

shows the average KER (fwhm) of selected photoions of the valence and core-excited  $\text{CH}_2\text{Cl}_2$  molecule as a function of the incident photon energy, where the influence of the transitions represented by band A and band B on the average KER of the  $\text{C}^+$ ,  $\text{CH}_2^+$ , and  $\text{Cl}^+$  cations can be seen. The Cl ( $2p_{1/2} \rightarrow 10a_1^*$ ) transition at 202.8 eV induces a full atomization breakup of the molecule and a sharp drop in the average KER of the  $\text{C}^+$  cations is observed. On the other hand, the Cl ( $2p_{3/2} \rightarrow 10a_1^*$ ) transition at 200.7 eV leads to a less pronounced decrease of the average KER of the  $\text{CH}_2^+$  cations. However, when the heavier  $\text{Cl}^+$  cations are ejected, both transitions reduce the average KER with similar strengths, leading to a shallower and wider KER decline.

It was observed that the fwhm for the  $\text{CH}_2^+$  and  $\text{Cl}^+$  fragments' TOF profiles are narrower at the Cl ( $2p_{3/2} \rightarrow 10a_1^*$ ) resonance, while the peak widths for the lighter  $\text{H}^+$ ,  $\text{H}_2^+$ ,  $\text{C}^+$ , and  $\text{CH}^+$  fragments are broader. Because the mass of the photoelectron is very small in comparison to the mass of the ion, the whole energy available in the process is essentially converted to electron kinetic energy. All fragments exhibit a considerable increase in the KER for excitation to molecular orbitals near the Cl  $2p_{3/2,1/2} \rightarrow \infty$  (IP).

From Figure 4, one can see that the KER of the  $\text{CH}_2^+$  ion presents a minimum at the Cl ( $2p_{3/2} \rightarrow 10a_1^*$ ) resonance. However, it was previously observed<sup>10</sup> that the  $\text{CH}_2^+$  ion yield (ion production) presents a maximum at the Cl ( $2p_{3/2} \rightarrow 10a_1^*$ ) resonance, which was interpreted by Lu et al.<sup>20</sup> as due to a fast dissociation through a highly repulsive potential curve. Thus, due to the fast dissociation process, the photoelectron takes most of the KER, due to its lower mass. Here we present calculations of the potential curves in order to give support to this assertion. Figure 5 shows the profile of energy versus C–Cl distance for the inner-shell singlet Cl ( $2p \rightarrow 10a_1^*$ ) neutral state. It is quite evident that the curve is repulsive and can promote fast dissociation. Such a process was suggested for methyl chloride,<sup>21</sup> and consists of dissociation of the nuclear framework before Auger decay, which takes place in the atom. It is worth emphasizing that for a given C–Cl distance all other molecular coordinates are optimized. Therefore, this is a minimum energy path to that state. For the state Cl ( $2p \rightarrow \infty$ ), an inner-shell single ionization, a similar profile is obtained as also included in Figure 5. A noticeable difference is the presence of a shallow minimum around 3.5 Å. In what concerns the discussion here, this difference is not relevant and an effective repulsive curve is also obtained. So, the process of ultrafast dissociation  $\text{CH}_2\text{Cl} + \text{Cl}^+$  is quite likely via the inner-shell curve.

Significant differences in the KER of the  $\text{CH}_2\text{Cl}_2$  fragments can be also observed from Figure 4 for the  $2p_{3/2} \rightarrow 10a_1^*$  and  $2p_{1/2} \rightarrow 10a_1^*$  transitions. This can be ascribed to the different symmetries of final states (they correspond to different states of the spin manifold). After excitation to these states, the molecule decays via resonant Auger decay. As Auger processes are mainly driven by Coulombic interaction, their transition probability is given by

$$M_{m'} = \left\langle n' \left| \frac{1}{r_{ij}} \right| n \right\rangle \quad (3)$$

where  $n$  and  $n'$  stand for initial and final states, respectively. It is worth emphasizing that those states can have discrete and continuum parts. In the present case, the Coulombic repulsion operator transforms the totally symmetric irreducible repre-

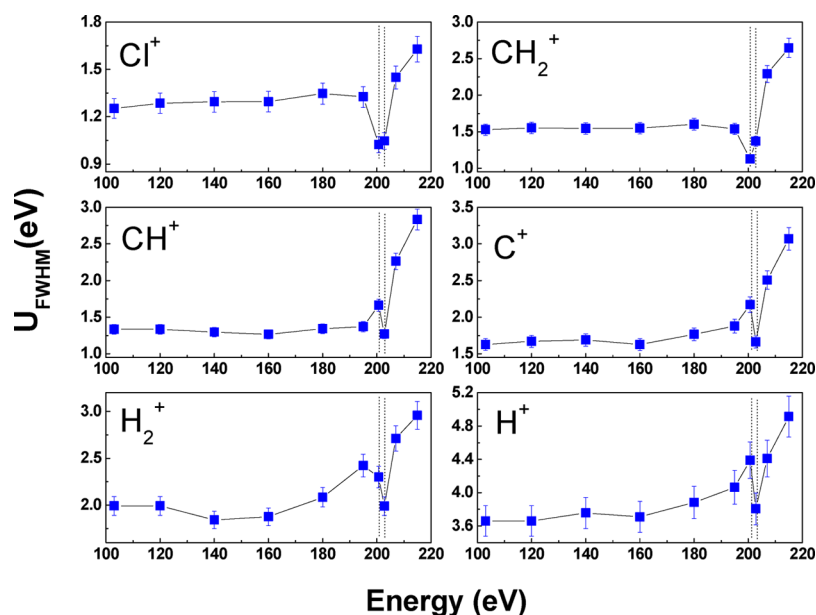


**Figure 4.** Average center-of-mass KER (fwhm) of some fragments of the  $\text{CH}_2\text{Cl}_2$  molecule as a function of the incident photon energy. The lines at 200.7 eV ( $2P_{3/2} \rightarrow 10a_1^*$ ) and 202.8 eV ( $2P_{1/2} \rightarrow 10a_1^*$ ) indicate the energy transitions.

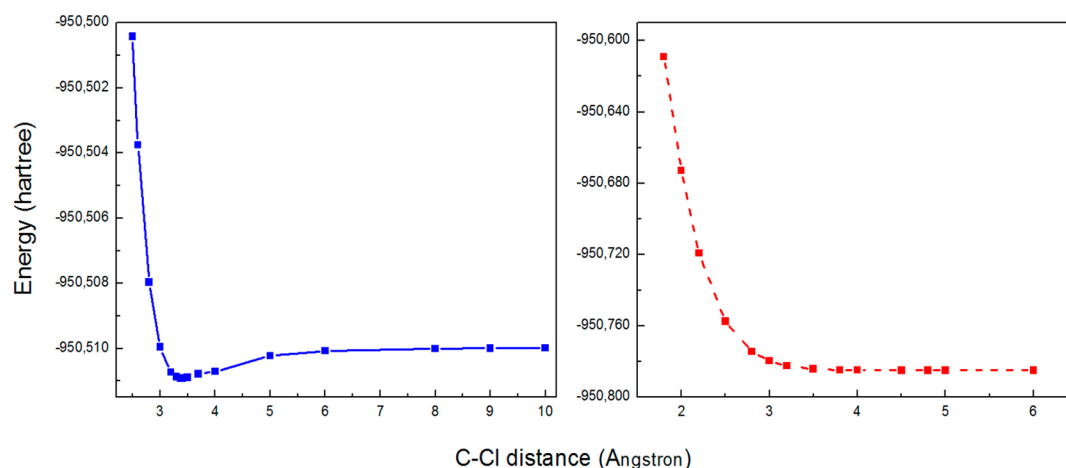


**Figure 5.** Potential curves for inner-shell singlet Cl ( $2p \rightarrow 10a_1^*$ ) excited state, represented by dashed red lines (right) and Cl ( $2p \rightarrow \infty$ ) ionized state, represented by full blue line (left). The total energy is calculated along the C–Cl distance. Each point represents the minimum energy, i.e., that obtained by optimization of the other nuclear coordinates.

sensation of the double  $C_{2v}$  group. In order to determine if transition probabilities are different from zero, one should examine the representation to which  $|n\rangle$  and  $|n'\rangle$  (or  $\langle n' |$ ) belongs. The product of their irreducible representations should contain the totally symmetric representation. Since the initial states are different; the value obtained in eq 3 is different in each case. Therefore, it is not surprising to verify that the fragmentation is strongly dependent on the generated initial core state, since each state will follow specific Auger decay and consequently different fragmentation processes.

Kinetic energy distributions for the  $\text{H}^+$  photodissociation fragments obtained at various photon energies are shown in Figure 6. The inset in Figure 6 displays the average KER obtained for the peak widths (fwhm) for comparison. The spectra show a sudden increase from 0 to around 5 eV, and drop more slowly after the maximum to 10% of their maximum intensity at 20 eV. The maximum kinetic energy value of the  $\text{H}^+$  fragments reaches 25 eV. Since the extraction field chosen for

the spectrometer in this experiment is high enough to guarantee 100% collection efficiency for ions up to 30 eV, this abrupt cutoff cannot be attributed to sharply decreasing collection efficiency. The high-energy components in the  $\text{H}^+$  KERD might be associated with aborted double ionization events that are included in the PEPICO spectra. The spectrum obtained at 195 eV shows a peak at the 4.5 eV kinetic energy. Around the Cl 2p edge and above, the KERD peak is located at 5.5 eV. The average KER shows a different behavior, increasing from 4.0 eV below the edge, exhibiting a minimum of 3.8 eV at the  $2P_{1/2} \rightarrow 10a_1^*$  resonance (202.8 eV), and increasing again above the edge to 4.9 eV.

The KERD of  $\text{C}^+$ , which corresponds to the full atomization of the molecule, can be discerned in Figure 7. In this case, a different tuning of the incident photon energy induces substantial KERD differences.

The structures in the KERD cannot be directly interpreted univocally due to the lack of theoretical potential energy curves

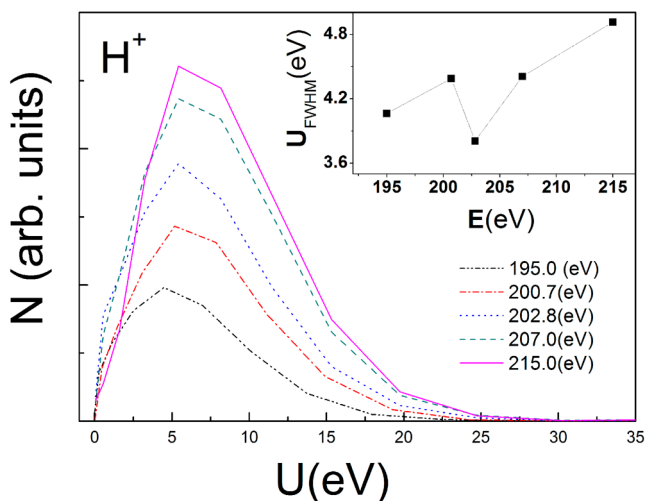


**Figure 6.** Center of mass KERD for the  $\text{H}^+$  ion at selected photon energies around the Cl 2p edge. The corresponding average (fwhm) values are displayed as inset as a function of the photon energy  $E$ . The vertical scale was arbitrarily chosen for each distribution. Note that, despite this arbitrary choice regarding the vertical scale, this has not affected the value of  $U_{\text{fwhm}}$  that is plotted in the inset. Due to the high number of counts (above  $2.5 \times 10^8$  for one single channel in the case of  $\text{H}^+$ ), the error bars are very small (well below 1% around the maxima of the KERD) and are not represented in the KERD.

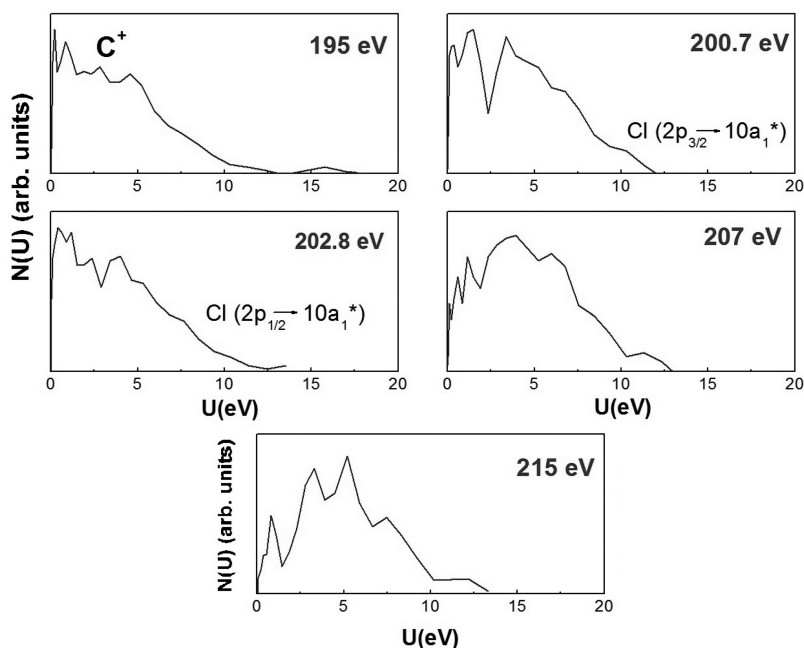
of the parent ion. In a simple picture of instantaneous dissociation into several atomic fragments, the  $\text{C}^+$  ions would hold very low kinetic energy due to its central position in the molecule. Notwithstanding, the measured translational KER of  $\text{C}^+$  is not negligible. Then, it is evident that these non-negligible parts in the  $\text{C}^+$  KER spectra (see Figure 4) are not cohesive with the scenario of a concerted rupture of all bonds. One possibility is that the  $\text{C}^+$  fragments are generated in a bent conformation, which, upon atomization, gives rise to  $\text{C}^+$

fragment ions having significant KER. The vibrational bending modes of the molecule could likewise transfer a certain amount of KER. Finally, a sequential dissociation might also occur, where a sequential bond breaking takes place. The spectra display richer structures. For instance, below the Cl 2p edge, at 195 eV, the KERD presents bands at 0.21, 0.84, 2.8, and 4.6 eV, and a tail on the high-energy side superimposed by a peak at 16 eV. This long tail implies the presence of a repulsive potential contributing to the formation of  $\text{C}^+$  + neutrals in the Franck–Condon region. The rich structures and the large width of the KERDs show that there are several potential energy curves that are actually populated in the excitation process.

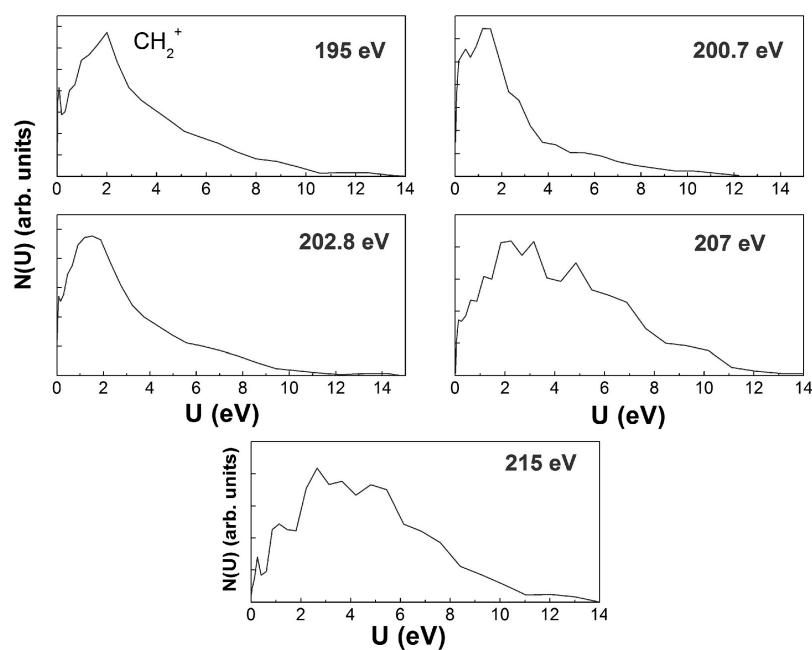
Figure 8 shows the KERD for the  $\text{CH}_2^+$  fragment. The  $\text{CH}_2^+$  KER spectra exhibit a small peak near zero eV and a maximum below 2 eV that moves to higher KER and becomes broader as the photon energy increases. Near the  $\text{CH}_2\text{Cl}_2$  ionization energy and above, the spectra exhibit structures, which can be interpreted as due to the opening of several dissociative states of  $\text{CH}_2\text{Cl}_2^+$ , which evidence themselves in the KERD. The maximum KER lies between 12 and 14 eV, depending on the photon energy, as shown above in Figure 4.

Figure 9 displays the KERD for the  $\text{Cl}^+$  fragment. The decreasing KERD for the heavier fragments is a consequence of the momentum conservation. At 195 eV, there are peaks centered at kinetic energies of 0.13, 0.51, and 0.97 eV, an intense peak centered at approximately 2.0 eV and a shoulder around 2.6 eV. The maximum translational energy is noted about 5 eV. At 200.7 eV, there are structures centered at 0.21, 0.68, 1.2, 2.1, 3.6, and 5.1 eV. At this energy, the average KER (see again Figure 9) decreases to about 0.18 eV. It can be seen that the KERDs of the  $\text{Cl}^+$  fragment show a sharp increase in intensity from 0 to 0.2 eV at 195, 200.7, and 202.8 eV photon energies, while at 207 and 215 eV, this feature is less pronounced.

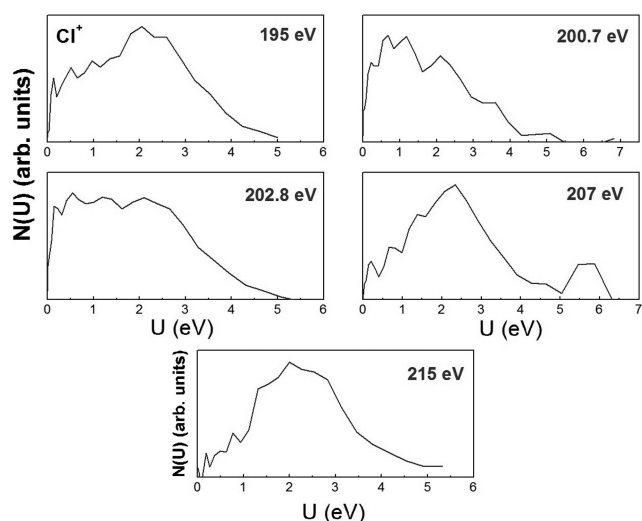
**IV.2. Dication  $\text{CH}_2\text{Cl}_2^{2+}$ .** Molecular dications are richer in electronic excited states in comparison to the isoelectronic



**Figure 7.** KERD for the  $\text{C}^+$  ion at selected photon energies around the Cl 2p edge. Due to the very good statistics, the observed structures are real and not due to experimental artifacts. The estimated error bars are below 1% around the maxima of the KERD.



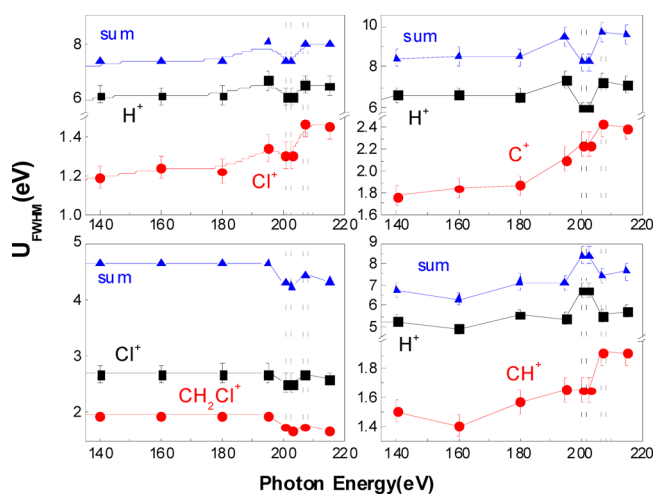
**Figure 8.** KERD for the  $\text{CH}_2^+$  ion at selected photon energies around the Cl 2p edge. Due to the very good statistics, the observed structures are considered to be real and not due to experimental artifacts.



**Figure 9.** KERD for the  $\text{Cl}^+$  ion at selected photon energies around the Cl 2p edge.

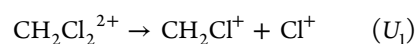
atomic dications because of their lower symmetry.<sup>22</sup> The fragmentation of the  $\text{CH}_2\text{Cl}_2^{2+}$  gives rise, preferentially, to the formation of two singly charged fragments. Neglecting the internuclear charge density effects,<sup>22</sup> the internuclear potential surface energy can be approximated by the Coulomb interaction between the fragment ions, of the charged fragments results in a larger KER. Besides its importance for electron correlation knowledge,<sup>11</sup> double photoionization of molecules has the particularity that the Franck–Condon transition from the neutral give rise to doubly charged moieties in a nuclear arrangement frequently exceedingly far from the nuclear equilibrium. Consequently, doubly charged polyatomic cations coming from double photoionization are commonly unstable moieties, which can dissociate into fragments with high kinetic energies, leading to striking results.<sup>23–25</sup> The average KERs of several dissociation channels of the doubly

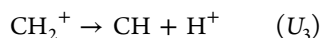
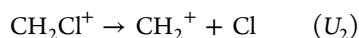
charged  $\text{CH}_2\text{Cl}_2^{2+}$  molecule are shown in Figure 10 as a function of the photon energy. The corresponding average KER



**Figure 10.** Average KER (fwhm) of some coincidences after double ionization of the  $\text{CH}_2\text{Cl}_2$  molecule as a function of the incident photon energy. The vertical lines indicate the positions of the transitions: Cl ( $2p_{3/2} \rightarrow 10a_1^*$  - 200.7 eV), Cl ( $2p_{1/2} \rightarrow 10a_1^*$ ), and ( $2p_{3/2} \rightarrow 10a_1^*$ ) (at 202.3 eV). The last two vertical lines indicate the Cl  $2p_{3/2,1/2}$  ionization potentials (206.4 eV) and (208.0 eV).

and KERDs were extracted after projecting the PE2PICO coincidences onto the  $T_1$  and  $T_2$  axes.<sup>11</sup> Due to momentum conservation, the lighter fragments carry larger KERs. It can be seen that the average KER for the  $\text{H}^+ + \text{Cl}^+$  coincidence are narrower at both  $2p_{3/2}$  and  $2p_{1/2}$  resonances. In contrast, the peak widths for the  $\text{H}^+ + \text{CH}^+$  coincidence are broader at those resonances. Below the Cl 2p resonance, the ratio of the momenta of  $\text{H}^+$  and  $\text{Cl}^+$  is  $p_{\text{H}^+}/p_{\text{Cl}^+} = -2.6$ , which is compatible with a four-body secondary decay<sup>26</sup>





In the case of the dissociation of the  $\text{CH}_2\text{Cl}_2^+$ , the predominant part of the KER is produced during charge separation. In that case, the KER can be approximately related to the nuclear distance between the fragments at the moment of the explosion,  $R$ , through the equation

$$U \text{ (eV)} = \frac{14.4q_1q_2}{R(\text{\AA})} \quad (4)$$

The neutral molecule ( $C_{2v}$ ) geometries are<sup>27,28</sup>  $R(\text{C}-\text{H}) = 1.78 \text{ \AA}$ ,  $R(\text{C}-\text{Cl}) = 1.77 \text{ \AA}$ ,  $\angle\text{HCH} = 112.0^\circ$ , and  $\angle\text{ClCCl} = 11.8^\circ$ . Based on eq 4 and Figure 10, one can estimate  $R \approx 2.0 \text{ \AA}$ .

In the case of the  $\text{H}^+ + \text{C}^+$  coincidence, the sum of the KER of both fragments lies between 8.3 and 9.7 eV, slightly larger than in the case of the former channel. This can be understood in terms of a smaller internuclear distance between the  $\text{H}^+$  and  $\text{C}^+$  fragments, since carbon is the central atom. In the case of the  $\text{Cl}^+ + \text{Cl}^+$  coincidence (not shown), both chlorine cations carry KER between 0.6 and 1.0 eV. They have the same KER (and the same momenta) only at the  $2p_{1/2}$  and  $2p_{3/2}$  resonances, indicating they are released in a secondary decay.<sup>26</sup>

The  $\text{CH}_2\text{Cl}^+ + \text{Cl}^+$  channel is usually considered as a Coulomb explosion process where, due to momentum conservation, the lighter fragment takes most of the energy. The validity of the assumption that the process  $\text{CH}_2\text{Cl}_2^{2+} \rightarrow \text{CH}_2\text{Cl}^+ + \text{Cl}^+$  is governed by a simple Coulomb explosion is evidenced by calculating the ground state potential curve, shown in Figure 11. For a distance larger than 2.85 Å, the curve is repulsive, while for smaller distances there is a potential well. This means that the dication can dissociate by Coulomb explosion or can have a longer lifetime depending on the region in which it is formed. As this state is formed from a repulsive inner-shell state, which can lead to fast dissociation, it is plausible to admit that it will be predominantly formed in the

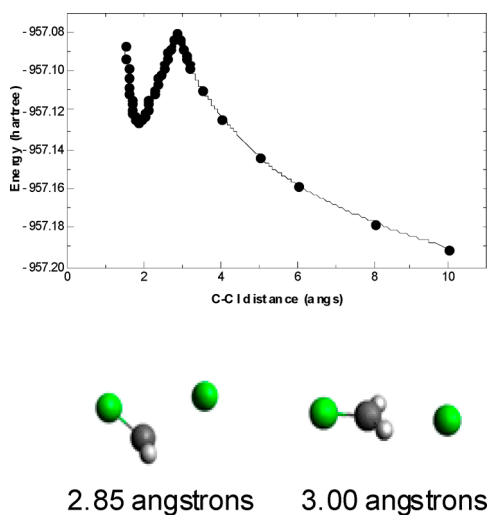


**Figure 11.** Top: potential energy curve for the ground state of dication  $\text{CH}_2\text{Cl}_2^{2+}$ . The total energy is calculated along the C–Cl distance. Each point represents the minimum energy, obtained by optimization of the other nuclear coordinates. Bottom: two selected configurations of the molecule at two different points of potential curve are shown: at 3.00 Å, the atoms are all in the same plane, while at 2.85 Å, a chlorine atom is out-of-plane, in a bonding-favoring geometry.

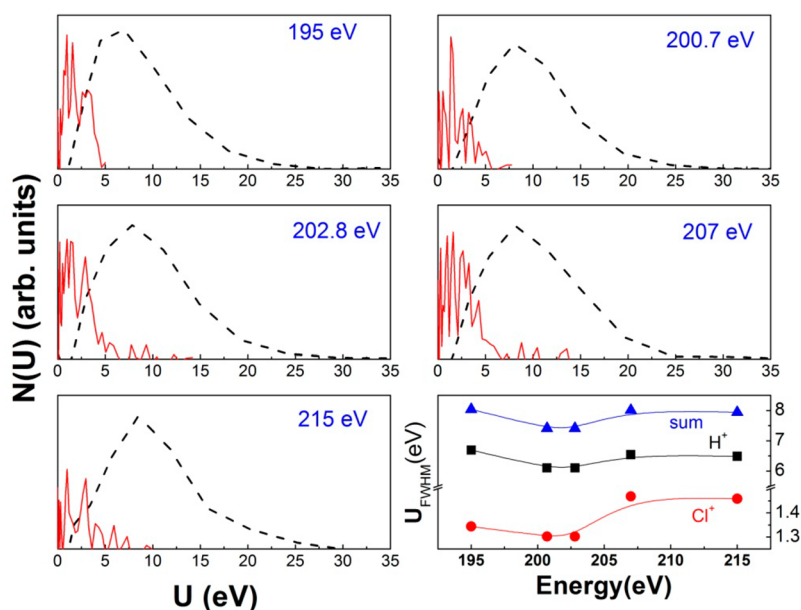
repulsive region, i.e., at distances larger than 2.85 Å. In fact, from eq 4 and Figure 10, one estimates that  $\text{CH}_2\text{Cl}^+ + \text{Cl}^+$  moieties are created at 3.2 Å. Thus, the assumption of pure Coulombic repulsion used above is justifiable. It is worth emphasizing the abrupt change of tendency of the potential curve at 2.85 Å. For larger distances, the  $\text{Cl}^+$  approaches  $\text{CH}_2\text{Cl}^+$  in plane with the two chlorine atoms at maximum distance. At shorter distances, the most stable approach is out-of-plane, which favors bonding. This is also shown in Figure 11. We can also estimate the lifetime of the  $\text{CH}_2\text{Cl}_2^{2+}$  dication. In fact, from eq 4, and Figures 10 and 11, in analogy to a square well,<sup>29</sup> the well and barrier widths are estimated as  $L \approx 0.8 \text{ \AA}$  and  $x \approx 0.7 \text{ \AA}$ , respectively. The penetration depth of the wave function is estimated as  $\delta \approx 4 \times 10^{-3} \text{ \AA}$ , and the tunnelling probability ( $T \approx \exp(-x/\delta)$ ) is estimated to be close to 100%. Thus, the lifetime ( $\tau \approx (L/v)T^{-1}$ ) is about 6.6 fs.

Figure 12 shows the KER distributions of the  $\text{H}^+ + \text{Cl}^+$  dissociation channel arising from the fragmentation of the  $\text{CH}_2\text{Cl}_2^{2+}$  precursor ion at selected photon energies around the Cl 2p edge. The measured  $\text{H}^+$  ion KERD is very broad and described by a single peak located around 7.5 eV at  $h\nu = 195 \text{ eV}$ , and rises as the photon energy increases, while, as expected, in single coincidence the peaks were observed around 5.5 eV (Figure 4). Both fragments present minimum average KER at the Cl 2p resonances. If we compare the average total energy values shown in Figure 10 with the theoretical KER values obtained from eq 4 using typical internuclear distances (2.0 Å), a fairly good agreement between experimental and theoretical values is achieved. The shape of the KERD profile of the  $\text{H}^+$  moiety changes slightly as a function of the photon energy. The maximum KERD of the  $\text{H}^+$  increases from 27 eV at  $h\nu = 195 \text{ eV}$  up to 30 eV at  $h\nu = 215 \text{ eV}$ . The KERD spectra of the  $\text{Cl}^+$  fragment show several narrow peaks.

Figure 13 displays the KERD of the  $\text{CH}_2^+ + \text{Cl}^+$  fragmentation channel arising from the fragmentation of the parent molecule dication as precursor ion at selected photon energies around the Cl 2p edge. Both distributions present several structures. Again, the structures observed in the distributions are not presently amenable to unambiguous interpretation due to the unavailability of detailed potential energy curves of the doubly charged DCM molecule. Notwithstanding, as opposed to the other channels, the dissociation channel is formed via a non-Coulomb potential energy curve. A two-step model has been postulated in the literature<sup>30</sup> in which initial excitation of very highly charged molecular states are followed by rapid dissociation.

## V. SUMMARY

A systematic experimental and theoretical study of the excitation and fragmentation processes of the  $\text{CH}_2\text{Cl}_2$  molecule was performed by the translational energy analysis of the ion fragments from the TOF peak shapes. Average KER and KERD are reported for the most abundant fragments in the PEPICO ( $\text{Cl}^+$ ,  $\text{H}^+$ , and  $\text{CH}_2^+$ ) and PE2PICO ( $\text{H}^+ + \text{Cl}^+$ ,  $\text{H}^+ + \text{C}^+$ ,  $\text{Cl}^+ + \text{Cl}^+$ , and  $\text{H}^+ + \text{CH}^+$ ) spectra, the latter arising from incomplete Coulomb fragmentation. In the photon energy range selected in this investigation, the increase of the photon energy evolves in an accompanying change in the KERDs, either in intensity or kinetic energy shift, comprising very different processes. The  $\text{H}^+$  fragment having the  $\text{CH}_2\text{Cl}_2^+$  as a precursor is ascertained to have a unimodal kinetic energy dispersion in the range from 0 to 20 eV, with a maximum kinetic energy near 5.0 eV. Significant differences in the KER of



**Figure 12.** KERD and average KER for the  $\text{H}^+ + \text{Cl}^+$  coincidence ions at selected photon energies around the Cl 2p edge. Dash lines:  $\text{H}^+$ ; solid lines:  $\text{Cl}^+$ .

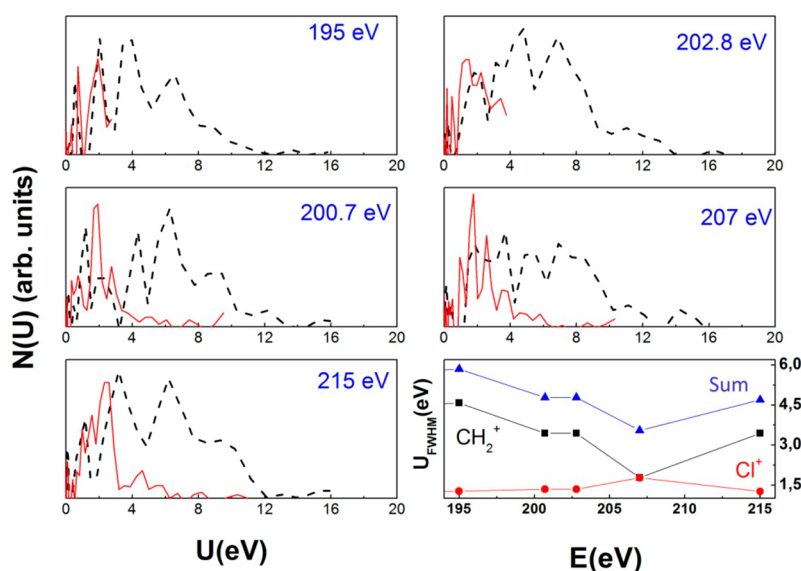


**Figure 13.** KERD and average KER for the  $\text{CH}_2^+ + \text{Cl}^+$  coincidence ions at selected photon energies around the Cl 2p edge. Dash lines:  $\text{CH}_2^+$ ; full lines:  $\text{Cl}^+$ .

the  $\text{CH}_2\text{Cl}_2$  fragments for the  $2\text{P}_{1/2} \rightarrow 10\text{a}_1^*$  and  $2\text{P}_{3/2} \rightarrow 10\text{a}_1^*$  transitions were observed and ascribed to the different symmetries of these states. Finally, catalytic cycles involving chlorine compounds are efficient sources of stratospheric chlorine. Chlorine atoms and ions participate in the catalytic ozone destruction, in which the speed of reaction depends strongly on the temperature and particle kinetic energy. Thus, we hope that the present study will shed some new light on the processes that contribute to the ozone depletion in atmosphere, as well as to contribute to the present knowledge about the dynamics of dissociation of polyatomic molecules near resonances.

## AUTHOR INFORMATION

### Corresponding Author

\*E-mail: [toni@if.ufrj.br](mailto:toni@if.ufrj.br). Phone: +55 21 3938-7947.

## Notes

The authors declare no competing financial interest.

## ACKNOWLEDGMENTS

This work is supported in part by CNPq and FAPERJ (Brazil). The authors thank M. MacDonald (CLS) for his valuable comments.

## REFERENCES

- (1) Singh, R.; Bhatt, P.; Yadav, N.; Shanker, R. Ionic Fragmentation of a  $\text{CH}_4$  Molecule Induced by 10-keV Electrons: Kinetic-Energy-Release Distributions and Dissociation Mechanisms. *Phys. Rev. A: At, Mol., Opt. Phys.* **2013**, *87*, 062706.
- (2) Singh, R.; Bhatt, P.; Yadav, N.; Shanker, R. Ionic Fragmentation of the CO Molecule by Impact of 10-keV Electrons: Kinetic-Energy-

Release Distributions. *Phys. Rev. A: At., Mol., Opt. Phys.* **2013**, *87*, 022709.

(3) Mathur, D. Structure and Dynamics of Molecules in High Charge States. *Phys. Rep.* **2004**, *391*, 1–118.

(4) Santos, A. C. F.; Melo, W. S.; Sant'Anna, M. M.; Sigaud, G. M.; Montenegro, E. C. Fragmentation and Mean Kinetic Energy Release of the Nitrogen Molecule. *Nucl. Instrum. Methods Phys. Res., Sect. B* **2007**, *261*, 200–203.

(5) Ravi, R.; Philip, L.; Swaminathan, T. Comparison of Biological Reactors (Biofilter, Biotrickling Filter and Modified RBC) for Treating Dichloromethane Vapors. *J. Chem. Technol. Biotechnol.* **2010**, *85*, 634–639.

(6) Hussain, M. A.; Ford, R.; Hill, J. Determination of Fecal Contamination Indicator Sterols in an Australian Water Supply System. *Environ. Monit. Assess.* **2010**, *165*, 147–157.

(7) Lu, H.; Zhu, L.; Chen, S. Pollution Level, Phase Distribution and Health Risk of Polycyclic Aromatic Hydrocarbons in Indoor Air at Public Places of Hangzhou, China. *Environ. Pollut.* **2008**, *152*, 569–575.

(8) Leedham Elvidge, E. C.; Oram, D. E.; Laube, J. C.; Baker, A. K.; Montzka, S. A.; Humphrey, S.; O'Sullivan, D. A.; Brenninkmeijer, C. A. M. Increasing Concentrations of Dichloromethane, CH<sub>2</sub>Cl<sub>2</sub>, Inferred from CARIBIC Air Samples Collected 1998–2012. *Atmos. Chem. Phys.* **2015**, *15*, 1939.

(9) Alcantara, K. F.; Wolff, W.; Gomes, A. H. A.; Sigaud, L.; Soriano, S.; Oliveira, V.; Rocha, A. B.; Santos, A. C. F. Fragmentation of the CH<sub>2</sub>Cl<sub>2</sub> Molecule by Proton Impact and VUV Photons. *J. Phys. B: At., Mol. Opt. Phys.* **2011**, *44*, 165205.

(10) Alcantara, K. F.; Gomes, A. H. A.; Wolff, W.; Sigaud, L.; Santos, A. C. F. Strong Electronic Selectivity in the Shallow Core Excitation of the CH<sub>2</sub>Cl<sub>2</sub> Molecule. *J. Phys. Chem. A* **2015**, *119*, 8822–8831.

(11) Alcantara, K. F.; Gomes, A. H. A.; Wolff, W.; Sigaud, L.; Santos, A. C. F. Outer-Shell Double Photoionization of CH<sub>2</sub>Cl<sub>2</sub>. *Chem. Phys.* **2014**, *429*, 1–4.

(12) Gomes, A. H. A.; Wolff, W.; Ferreira, N.; Alcantara, K. F.; Luna, H.; Sigaud, G. M.; Santos, A. C. F. Deep Core Ionic Photo-fragmentation of the CF<sub>2</sub>Cl<sub>2</sub> Molecule. *Int. J. Mass Spectrom.* **2012**, *319*–*320*, 1–8.

(13) Santos, A. C. F.; Homem, M. G.; Almeida, D. P. Production of Highly Charged Ne Ions by Synchrotron Radiation. *J. Electron Spectrosc. Relat. Phenom.* **2011**, *184*, 38–42.

(14) Rocha, A. B. Spin-Orbit Splitting for Inner-Shell 2p States. *J. Mol. Model.* **2014**, *20*, 2349–2355.

(15) Bethe, H. A.; Salpeter, E. E. *Quantum Mechanics of the One and Two Electron Atoms*; Plenum: New York, 1977.

(16) Furlani, T. R.; King, H. F. Theory of Spin-Orbit Coupling. Application to Singlet–Triplet interaction in the Trimethylene Biradical. *J. Chem. Phys.* **1985**, *82*, 5577.

(17) Fedorov, D. G.; Gordon, M. S. A Study of the Relative Importance of One and Two-Electron Contributions to Spin–orbit Coupling. *J. Chem. Phys.* **2000**, *112*, 5611.

(18) Berning, A.; Schweizer, M.; Werner, H.-J.; Knowles, P. J.; Palmieri, P. Spin-Orbit Matrix Elements for Internally Contracted Multireference Configuration Interaction Wavefunctions. *Mol. Phys.* **2000**, *98*, 1823–1833.

(19) Werner, H.-J.; Knowles, P. J.; Knizia, G.; Manby, F. R.; Schütz, M., et al. *MOLPRO*, v 2012.1, A Package of Ab Initio Programs; <http://www.molpro.net>.

(20) Lu, K. T.; Chen, J. M.; Lee, J. M.; Haw, S. C.; Chen, S. A.; Liang, Y. C.; Chen, S. W. State-Selective Enhanced Production of Positive Ions and Excited Neutral Fragments of Gaseous CH<sub>2</sub>Cl<sub>2</sub> Following Cl 2p Core-Level Photoexcitation. *Phys. Rev. A: At., Mol., Opt. Phys.* **2010**, *82*, 033421.

(21) Miron, C.; Morin, P.; Céolin, D.; Journel, L.; Simon, M. Multipathway Dissociation Dynamics of Core-Excited Methyl Chloride Probed by High Resolution Electron Spectroscopy and Auger-Electron-Ion Coincidences. *J. Chem. Phys.* **2008**, *128*, 154314.

(22) Safvan, C. P.; Mathur, D. Dissociation of Highly Charged N<sub>2</sub><sup>q+</sup> ( $q \geq 2$ ) Ions via Non-Coulombic Potential Energy Curves. *J. Phys. B: At., Mol. Opt. Phys.* **1994**, *27*, 4073.

(23) Dujardin, G.; Winkoun, D.; Leach, S. Double Photoionization of Methane. *Phys. Rev. A: At., Mol., Opt. Phys.* **1985**, *31*, 3027.

(24) Thissen, R.; Witasse, O.; Dutuit, O.; Wedlund, C. S.; Gronoff, G.; Lilensten, J. Doubly-Charged Ions in the Planetary Ionospheres: A Review. *Phys. Chem. Chem. Phys.* **2011**, *13*, 18264–18287.

(25) Sigaud, L.; Ferreira, N.; Montenegro, E. C. Absolute Cross Sections for O<sub>2</sub> Dication Production by Electron Impact. *J. Chem. Phys.* **2013**, *139*, 024302.

(26) Simon, M.; Lebrun, T.; Martins, R.; de Souza, G. G. B.; Nenner, I.; Lavollee, M.; Morin, P. Multicoincidence Mass Spectrometry Applied to Hexamethyldisilane Excited around the Si 2p Edge. *J. Phys. Chem.* **1993**, *97*, 5228–5237.

(27) Grant, R. P.; Harris, F. M.; Parry, D. E. An Experimental and Computational Study of the Double Ionization of CH<sub>3</sub>Cl, CH<sub>2</sub>Cl<sub>2</sub>, and CHCl<sub>3</sub> Molecules to Singlet and Triplet Electronic States of Their Dications. *Int. J. Mass Spectrom.* **1999**, *192*, 111–123.

(28) Myers, R. J.; Gwinn, W. D. The Microwave Spectra, Structure, Dipole Moment, and Chlorine Nuclear Quadrupole Coupling Constants of Methylene Chloride. *J. Chem. Phys.* **1952**, *20*, 1420.

(29) Griffiths, D. J. *Introduction to Quantum Mechanics*, 2nd ed.; Prentice-Hall, 2005.

(30) Hill, W. T., III; Zhu, J.; Hatten, D. L.; Cui, Y.; Goldhar, J.; Yang, S. Role of Non-Coulombic Potential Curves in Intense Field Dissociative Ionization of Diatomic Molecules. *Phys. Rev. Lett.* **1992**, *69*, 2646.